Zhijia Dong, Dong Xia, Pibo Ma*, Gaoming Jiang

Warp-knitted Fabric Defect Segmentation Based on the Shearlet Transform

DOI: 10.5604/01.3001.0010.4633

Ministry of Education, Jiangnan University, Engineering Research Center for Knitting Technology,
Jiangsu, Wuxi, 214122, China
* E-mail: mapibo@jiangnan.edu.cn

Abstract
*The Shearlet transform has been a burgeoning method applied in the area of image processing recently which, differing from the Wavelet transform, has excellent properties in processing singularities for multidimensional signals. Not only is it similar to the performance of the Curvelet transform, it also overcomes the disadvantage of the Curvelet transform with respect to discretization. In this paper, the Shearlet transform with segmented threshold de-nosing is proposed to segment a warp-knitted fabric defect. Firstly a warp-knitted fabric image of size 512*512 is filtered by the Laplacian Pyramid transform and decomposed into low frequency and high frequency coefficients. Secondly the high frequency coefficients are operated with a pseudo-polar grid and then convoluted by the window function. Thirdly the shearlet coefficients will be obtained through redefining the Cartesian coordinates from the pseudo-polar grid coordinates and de-noised by the segmented threshold method. Then the coefficients which have high energy are selected for reconstruction in an inverse way using the previous steps. Finally the iterative threshold method and object operation based on morphology are applied to segment out the defect profile. The experiment's result states that the Shearlet transform shows excellent performance in segmenting a common warp-knitted fabric defect, indicating that the segment results can be applied for further defect automatic recognition.*

Key words: *warp-knitted fabric defect, Shearlet transform, Fourier transform, segmented threshold de-nosing.*

Introduction

Warp-knitted fabric, being a more and more extensively used material in social production and life, makes the yarn bend in a loop and draw it through the old loop [1]. With fiercer market competition, fabric quality is the pivotal issue to guarantee optimized benefits from fabric production. Fabric defect detection is an important part of quality assurance. In spite of the existence of artificial detection of fabric defects in small and mid-size companies, automated fabric defect detection is is a much talked about application in most districts. Traditionally the methods for fabric defect detection are divided into two approaches: the spatial domain method and frequency domain method. But in review [2], they are classified widely into seven types: statistical (Auto-correlation function [3], co-occurrence matrix [4], mathematical morphology [5], the fractal method [6]), the spectral wavelet transform [7], the Fourier transform [8], the Gabor transform [9]), the autoregressive model [10], Markov random fields [11]), learning neural networks [12], and structural [13], hybrid [14] and motif-based [15].

Most of the methods mentioned above are applied for woven fabric defect detection, but research on warp-knitted fabric defect detection is scarce. In order to meet the demand for warp-knitted fabric quality control, the burgeoning method of image processing is introduced. The method named the Shearlet transform is a flexible operator which combines geometry and multiscale analysis. It has excellent directional sensitivity and overcomes the shortcomings of dealing with distributed discontinuities such as edges in high-dimensional signals. Therefore it will have promising performance in the segmentation of the defect profile and is also widely applied in some applications like the extraction of texture features [27]. By using the Shearlet transform with segmented threshold de-nosing, this work segments some common defects in warp-knitted fabric, such as broken warp, oil and holes. The result shown in our work demonstrates that the Shearlet transform is an effective way of warp-knitted fabric defect partition, and the defect profile is distinct enough for further defect recognition.

Shearlet transform

The traditional Wavelet transform has the promising property of processing pointwise singularities for 1-D signals. But recently it is widely acknowledged that this property can be ineffective in distributing discontinuities, such as edges in high-dimensional signals. Therefore many methods for settling this matter have been proposed over the years, such as the complex Wavelet transform [16], Brushlet transform [17], Ridgelet transform [18], Curvelet transform [19], Contourlet transform [20] and Shearlet transform [21-22]. These methods have high direction sensitivity and are excellent for the representation of distributed discontinuities such as edges; however, for some of them it is difficult to implement the discretization of the transforms, which makes them not suitable for high-dimensional signals theoretically. However, the Shearlet transform overcomes this drawback and has more flexible decomposition for multiscale geometric analysis.

Theory of Shearlet transform

The Shearlet transform is constructed for multiscale geometric analysis by affine systems. In the dimension $d = 2$, the affine systems ξ with composite dilations can be defined as follows.

$$\zeta_{TS}(\psi) = \left\{ \psi_{l,n,k}(x) = |detT|^{l/2} \psi\left(S^n T^l x - k\right) : l, n \in Z, k \in Z^2 \right\} \quad (1)$$

Where ψ is a collection of the basis function; T denotes the anisotropy matrix for multi-scale partitions, S is a shear matrix for directional analysis; l, n and k are the scale, direction and translation parameters, respectively; T^l is used for scale transformation; S^n relates to geometrical transformation, and T & S are both 2×2 invertible matrices and $|B| = 1$. For both $a > 0$ and $b \in R$, the matrices of T and S are represented as:

$$T = \begin{bmatrix} a & 0 \\ 0 & \sqrt{a} \end{bmatrix}, S = \begin{bmatrix} 1 & b \\ 0 & 1 \end{bmatrix} \quad (2)$$

When $a = 2$, $b = 1$, ***Equation (2)*** is written as follows:

$$T = \begin{bmatrix} 4 & 0 \\ 0 & 2 \end{bmatrix}, T = \begin{bmatrix} 1 & 1 \\ 0 & 1 \end{bmatrix} \quad (3)$$

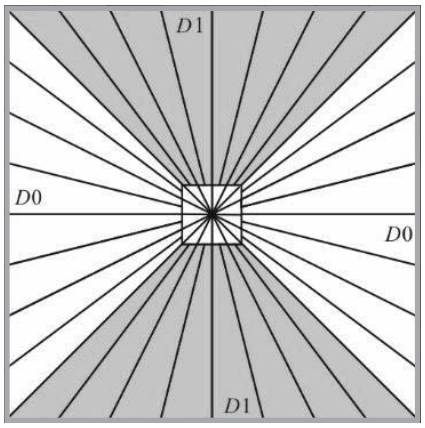

Figure 1. *Partition graph of the frequency plane by Shearlets.*

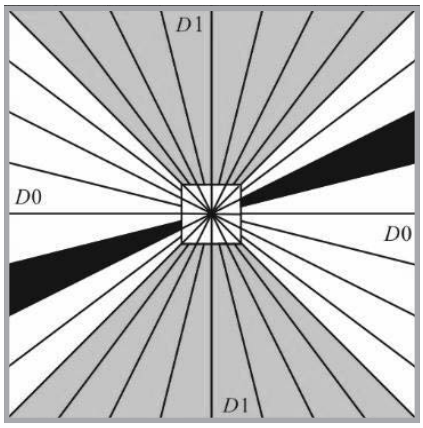

Figure 2. *Elements of the partition graph.*

Figure 1 shows a partition graph of the frequency plane by means of shearlets. The white region is illustrated as an horizontal cone D_0 and the blue region is considered as a vertical cone D_1. The frequency elements $\check{\psi}_{l,n,k}$ should be defined to construct the above cones, which is the result of the Fourier transform to $\psi_{l,n,k}$.

$$\check{\psi}_{l,n,k}(x) = |detT|^{-l/2}\,\psi\left(S^{-n}T^{-l}x\right)e^{2\pi ixS^{-n}T^{-l}k} \tag{4}$$

In addition, horizontal cone D_0 and vertical cone D_1 are associated with frequency elements $\check{\psi}^{(0)}_{l,n,k}$ and $\check{\psi}^{(1)}_{l,n,k}$ respectively.

The collection of shearlets at the horizontal cone D_0 can be constructed in the following steps. For any $\gamma = (\gamma_1, \gamma_2) \in \hat{R}^2$, $\gamma_1 \neq 0$, $\check{\psi}^{(0)}(\gamma)$ can be expressed as ***Equation (5)***.

$$\check{\psi}^{(0)}(\gamma) = \check{\psi}^{(0)}(\gamma_1,\gamma_2) = \check{\psi}_1(\gamma_1)\check{\psi}_2\left(\frac{\gamma_2}{\gamma_1}\right) \tag{5}$$

In this equation, $\check{\psi}_1$ and $\check{\psi}_2 \in R$. The supported region of $\check{\psi}_1$ is defined as $\left[-\frac{1}{2},-\frac{1}{16}\right]\cup\left[\frac{1}{16},\frac{1}{2}\right]$ and $\check{\psi}_2$ is $[-1,1]$. And then they can be assumed as follows.

$$\sum_{l\geq 0}\left|\check{\psi}_1\left(2^{-2l}\omega\right)\right|^2 = 1, |\omega| \geq \frac{1}{8} \tag{6}$$

$$\sum_{n=-2^l}^{2^l-1}\left|\check{\psi}_2\left(2^{2l}\omega - n\right)\right|^2 = 1, |\omega| \leq 1 \tag{7}$$

On account of ***Equations (6)*** and ***(7)***, $\check{\psi}^{(0)}(\gamma)$ has the formula as follows, where $(\gamma_1,\gamma_2) \in D_0$, and $D_0 = \left\{(\gamma_1,\gamma_2) \in \hat{R}^2 : |\gamma_1| \geq \frac{1}{8}, \left|\frac{\gamma_2}{\gamma_1}\right| \leq 1\right\}$.

Hence ***Equation (8)*** implies that function $\check{\psi}^{(0)}\left(T_0^{-l}S_0^{-n}\gamma\right)$ will construct the partition of cone D_0, as shown in ***Figure 1***.

Then the collection of shearlets at the horizontal cone D_0 can be illustrated by the following ***Equation (9)***.

$$\sum_{l\geq 0}\sum_{n=-2^l}^{2^l-1}\left|\check{\psi}^{(0)}\left(T_0^{-l}S_0^{-n}\gamma\right)\right|^2 = \sum_{l\geq 0}\sum_{n=-2^l}^{2^l-1}\left|\check{\psi}_1\left(2^{-2l}\gamma_1\right)\right|^2\left|\check{\psi}_2\left(2^{2l}\frac{\gamma_2}{\gamma_1} - n\right)\right|^2 = 1 \tag{8}$$

$$\left\{\psi^{(0)}_{l,n,k}(x) = 2^{3l/2}\psi^{(0)}\left(T_0^l S_0^n x - k\right) : l \geq 0, -2^l \leq n \leq 2^l - 1, k \in Z^2\right\} \tag{9}$$

$$\text{support}\,\check{\psi}^{(0)}_{l,n,k} \subset \left\{(\gamma_1,\gamma_2) : \gamma_1 \in \left[-2^{2l-1},-2^{2l-4}\right]\cup\left[2^{2l-4},2^{2l-1}\right], \left|\frac{\gamma_2}{\gamma_1} - n2^{-l}\right| \leq 2^{-l}\right\} \tag{10}$$

$$\left\{\psi^{(1)}_{l,n,k}(x) = 2^{3l/2}\psi^{(1)}\left(T_1^l S_1^n x - k\right) : l \geq 0, -2^l \leq n \leq 2^l - 1, k \in Z^2\right\} \tag{11}$$

$$f, \psi^{(E)}_{l,n,k} = 2^{3l/2}\int f(x)\psi^{(E)}_{l,n,k}(x)e^{-2\pi ixS_E^{-n}T_E^{-l}k}dx, E = 1, 0 \tag{12}$$

Equations (8), (9), (10), (11) *and* ***(12)***.

The collection is a Parseval frame and the support in the frequency domain of $\check{\psi}^{(0)}_{l,n,k}$ is defined by ***Equation (10)*** [23]. This means the frequency element of $\check{\psi}^{(0)}_{l,n,k}$ is supported by a pair of trapezoids as a black region, as shown in ***Figure 2***, and the area of the single trapezoid is of approximate size $2^{2l} \times 2^l$. Additionally the trapezoids are oriented along the lines of the slope n^{2-l}.

Similarly the collection of shearlets at the vertical cone D_1 is implied as follows ***Equation (11)***.

Finally the Shearlet transform of $f \in L^2(R^2)$ can be expressed as ***Equation (12)***.

In general, the shearlets construct a tight support flame in different scales and directions. Moreover an optimal representation for the distributed discontinuities like edges in images can be archived as well. Moreover the approximate error of shearlets satisfies ***Equation (13)*** to achieve the best approximation. Where C^2 is defined as the 2-D continuous differentiable function space and N illustrates the N largest coefficients in the shearlet expression.

$$\varepsilon_N \leq CN^{-2}\left(\log N\right)^3 \tag{13}$$

Implementation of discrete Shearlet transform in frequency domain

Traditionally the information from the images is discontinuous, and the collection of shearlets presented above is not appropriate to achieve a promising representation of the images. Thus the implementation of discretization for shearlets is essential. Theoretically the implementation of discretization for shearlets can be classified into two methods: the frequency domain and time domain. The frequency domain method is intuitionistic enough for the procedures of discretization and is adopted in this paper to implement the discretization of shearlets.

In order to realize the discretization for shearlets, a window function $W^{(D)}_{l,n}$ for decomposing the frequency plane is defined. $W^{(D)}_{l,n}$ is located on a pair of trapezoids and defined in terms of function ψ_2, illustrated as ***Equations (14)*** and ***(15)***.

Where $\gamma = (\gamma_1,\gamma_2) \in \hat{R}^2$, $\gamma_1 \neq 0$, l = 0, 1, 2, …n, Z and $n = -2^l, \ldots, 2^l - 1$, is the indicator function of set D. and $W^{(d)}_{l,n}$ satisfies the condition below, illustrated as ***Equation (16).***

$$\sum_{E=0}^{1}\sum_{n=-2^l}^{2^l-1}\left|W_{l,n}^{(E)}(\gamma_1,\gamma_2)\right|^2=1 \qquad (16)$$

Naturally the Fourier transform of shearlets $\psi_{l,n,k}$ in a discretization form can be obtained by ***Equation (17)***, where L(γ) is used for the acquistion of a high frequency signal and $\check{\mathrm{L}}(\gamma)=\mathrm{L}(\gamma_1,\gamma_2)=$ $=\check{\psi}_1(\gamma_1)\mathrm{H}_{D_0}(\gamma_1,\gamma_2)+\check{\psi}_1(\gamma_2)\mathrm{H}_{D_1}(\gamma_1,\gamma_2)$.

Eventually the Shearlet transform of $f\in L^2(R^2)$ can be illustrated as ***Equation (18).***

Let the input signal be a 2-D image f of size $N*N$, and the discrete Fourier transform of the image $f(\gamma_1,\gamma_2)$, the decomposition procedure of the image by Shearlet transform can be implemented by the steps below. The first step of the discrete Shearlet transform is to obtain high frequency coefficients of the image by using the Laplacian Pyramid transform (LPT).

The LPT decomposes the image into a low frequency coefficient containing essential information of the original image and a high frequency coefficient containing the image details [24]. The decomposition procedure of LPT is illustrated in ***Figure 3***, where D is the decomposition filter, C the synthesis filter, and M the sample matrix. In this decomposition procedure, the low frequency coefficient is obtained by processing the original image f with the decomposition filter and down-sampled matrix and then processed sequentially by the up-sampled matrix, synthesis filter and a prediction coefficient like the original one acquired. While the high frequency coefficient b is the D-value between the original image and prediction coefficient. Mathematically the decomposition can be simply expressed as ***Equation (19)***. Here the notation is same as that mentioned above.

$$\check{f}_d^{\,l}(\gamma_1,\gamma_2)=\check{f}(\gamma_1,\gamma_2)\overline{\mathrm{L}\left(2^{-2l}\gamma_1,2^{-2l}\gamma_2\right)} \qquad (19)$$

The high frequency coefficient $\check{f}_d^{\,l}(\gamma_1,\gamma_2)$ will be processed on a pseudo-polar grid which describes the samples in the frequency domain as along lines across the origin at different slopes [22]. And the pseudo-polar coordinates (z, c) are defined as follows:

$$(z,c)=\left(\gamma_1,\frac{\gamma_2}{\gamma_1}\right),\ if\ (\gamma_1,\gamma_2)\in D_0 \qquad (20)$$

$$(z,c)=\left(\gamma_2,\frac{\gamma_1}{\gamma_2}\right),\ if\ (\gamma_1,\gamma_2)\in D_1 \qquad (21)$$

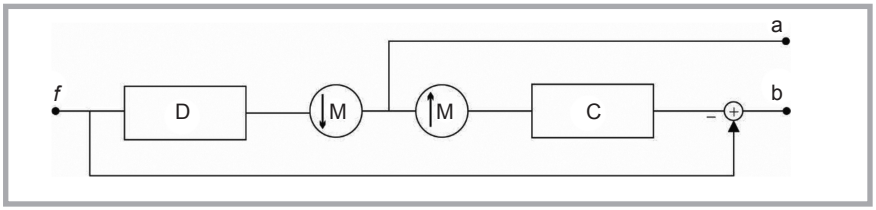

Figure 3. *Decomposition of the Laplacian Pyramid transform.*

Therefore the high frequency coefficient $\check{f}_d^{\,l}(\gamma_1,\gamma_2)$ can be redefined as $g_l(z,c)=$ $=\check{f}_d^{\,l}(\gamma_1,\gamma_2)=\check{f}(\gamma_1,\gamma_2)\overline{\mathrm{L}\left(2^{-2l}\gamma_1,2^{-2l}\gamma_2\right)}$. $g_l(z,c)$ will be filtered by the 1-D band-pass filter along axis c. The 1-D band-pass filter here is the discrete Fourier transform of window function $W_{l,n}^{(D)}$ and set as $\overline{W\left(2^l v-n\right)}$, where $n=-2^l,\ldots,2^l-1$.

Then the Shearlet coefficients $\left\langle f,\psi_{l,n,k}^{(0)}\right\rangle$ can be simply expressed as below based on ***Equation (18)***. It redefines the Cartesian coordinates from the pseudo-polar grid coordinates, and k_1, k_2 is the coordinate point of discrete samples of the high frequency coefficient. Similarly Shearlet coefficients at D_1 can be obtained in this way.

The sketch graph of the decomposition procedure of the Shearlet transform introduced above is also shown in ***Figure 4***, where *fa* and *fd* are the low frequency coefficient and high frequency coefficient, respectively, and W is the window function.

Defect segmentation

Decomposition with segmented threshold de-noising

Figure 5 shows a warp-knitted fabric defect gray image of size 512*512. With the implementation of the discrete Shearlet transform described in Section "Implementation of discrete Shearlet transform in frequency domain", the high frequency coefficient at every level can be divided into a number of shearlet coefficients. The key point to decompose the fabric image is the decomposition level.

In order to determine the level of decomposition, the edge information of the image should be taken into consideration. The sum of energy of the shearlet coefficients at the lth level is computed and then divided by the last level, as shown in equation (23); if $R_l>1$, the image should

$$W_{l,n}^{(0)}(\gamma)=\begin{cases}\check{\psi}_2\left(2^l\frac{\gamma_2}{\gamma_1}-n\right)\mathrm{H}_{D_0}(\gamma)+\check{\psi}_2\left(2^l\frac{\gamma_1}{\gamma_2}-n+1\right)\mathrm{H}_{D_1}(\gamma), & if\ n=-2^l\\ \check{\psi}_2\left(2^l\frac{\gamma_2}{\gamma_1}-n\right)\mathrm{H}_{D_0}(\gamma)+\check{\psi}_2\left(2^l\frac{\gamma_1}{\gamma_2}-n-1\right)\mathrm{H}_{D_1}(\gamma), & if\ n=2^l-1\\ \check{\psi}_2\left(2^l\frac{\gamma_2}{\gamma_1}-n\right), & otherwise\end{cases} \qquad (14)$$

$$W_{l,n}^{(1)}(\gamma)=\begin{cases}\check{\psi}_2\left(2^l\frac{\gamma_2}{\gamma_1}-n+1\right)\mathrm{H}_{D_0}(\gamma)+\check{\psi}_2\left(2^l\frac{\gamma_1}{\gamma_2}-n\right)\mathrm{H}_{D_1}(\gamma), & if\ n=-2^l\\ \check{\psi}_2\left(2^l\frac{\gamma_2}{\gamma_1}-n-1\right)\mathrm{H}_{D_0}(\gamma)+\check{\psi}_2\left(2^l\frac{\gamma_1}{\gamma_2}-n\right)\mathrm{H}_{D_1}(\gamma), & if\ n=2^l-1\\ \check{\psi}_2\left(2^l\frac{\gamma_1}{\gamma_2}-n\right), & otherwise\end{cases} \qquad (15)$$

$$\check{\psi}_{l,n,k}^{(E)}(\gamma)=2^{3l/2}\mathrm{L}\left(2^{-2l}\gamma\right)W_{l,n}^{(E)}(\gamma)e^{-2\pi i\gamma S_E^{-n}T_E^{-l}k},\ E=1,2 \qquad (17)$$

$$f,\psi_{l,n,k}^{(E)}=2^{3l/2}\int\check{f}(\gamma)\overline{\mathrm{L}\left(2^{-2l}\gamma\right)W_{l,n}^{(E)}(\gamma)}e^{2\pi i\gamma S_E^{-n}T_E^{-l}k}d\gamma,\ E=1,0 \qquad (18)$$

$$f,\psi_{l,n,k}^{(0)}=2^{-3l/2}\int g_l(z,c)\overline{W\left(2^l v-n\right)}exp\left(2\pi i\left(\frac{k_1+nk_2}{4^l}\gamma_1+\frac{k_2}{2^l}\gamma_2\right)\right)d\gamma_1 d\gamma_2 \qquad (22)$$

Equations (14), (15), (17), (18) *and* ***(22)***.

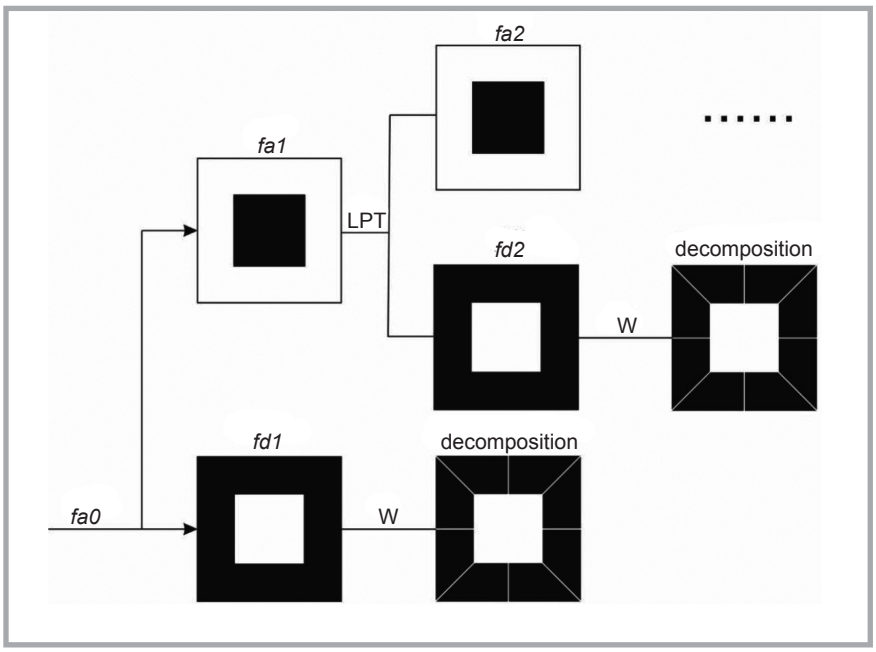

Figure 4. *Sketch graph of decomposition of the Shearlet transform.*

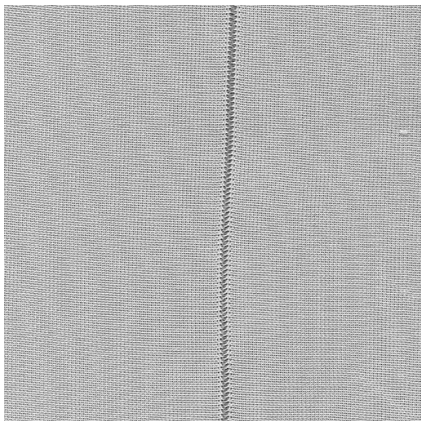

Figure 5. *Warp-knitted fabric with broken warp at the front bar.*

be decomposed again, otherwise the current level is the best. In our implementation, the best level is 4.

$$R_l = \frac{E_l^1 + E_l^2 + \ldots + E_l^n}{E_{l-1}^1 + E_{l-1}^2 + \ldots + E_{l-1}^{n'}} \qquad (23)$$

In the above equation, E_l^n is the energy of the the nth shearlet coefficient at the lth level and calculated as the square of the norm of the coefficient matrix $coef_l^n$, as shown in ***Equation (24)***.

$$E_l^n = coef_l^{n2}, l = 0,1,2,3; n = 1,2,3\ldots \qquad (24)$$

During the decomposition of the image by the Shearlet transform, the shearlet coefficients at every level are freewill, enabling the Shearlet transform to provide a more meticulous decomposition for the high frequency coefficient. In our work, the number of shearlet coefficients at every level is set as 10, 10, 18 and 18, respectively. ***Figures 6*** to ***9*** show the shearlet coefficients of the image at levels 1 to 4. Generally this meticulous decomposition means that much more directional information can be achieved in this procedure. However, not all the shearlet coefficients contain effective directional information, most of which are distributed with noise and need to be processed for the reconstruction, for which the segmented threshold de-nosing method is applied in this paper.

The coefficients acquired are classified into the signal noise coefficient, transition coefficient and signal coefficient based on the energy computed in ***Equation (24)***. The four shearlet coefficients that have the least energy at every level are identified as the noise coefficients in our work. The threshold de-noising method used is called as the Sqtwolog rule. The threshold T_l applied in the Sqtwolog rule is computed as ***Equation (25)***, where n is the number of total Shearlet coefficients at the operated level, and σ is the noise signal deviation. This method has the powerful property of de-noising and can get rid of most noise in shearlet coefficients.

$$T_l = \sigma\sqrt{2\ln n} \qquad (25)$$

Then the rest of the shearlet coefficients should be operated by other methods, and the average value E_A of the four shearlet coefficients mentioned above is comput-

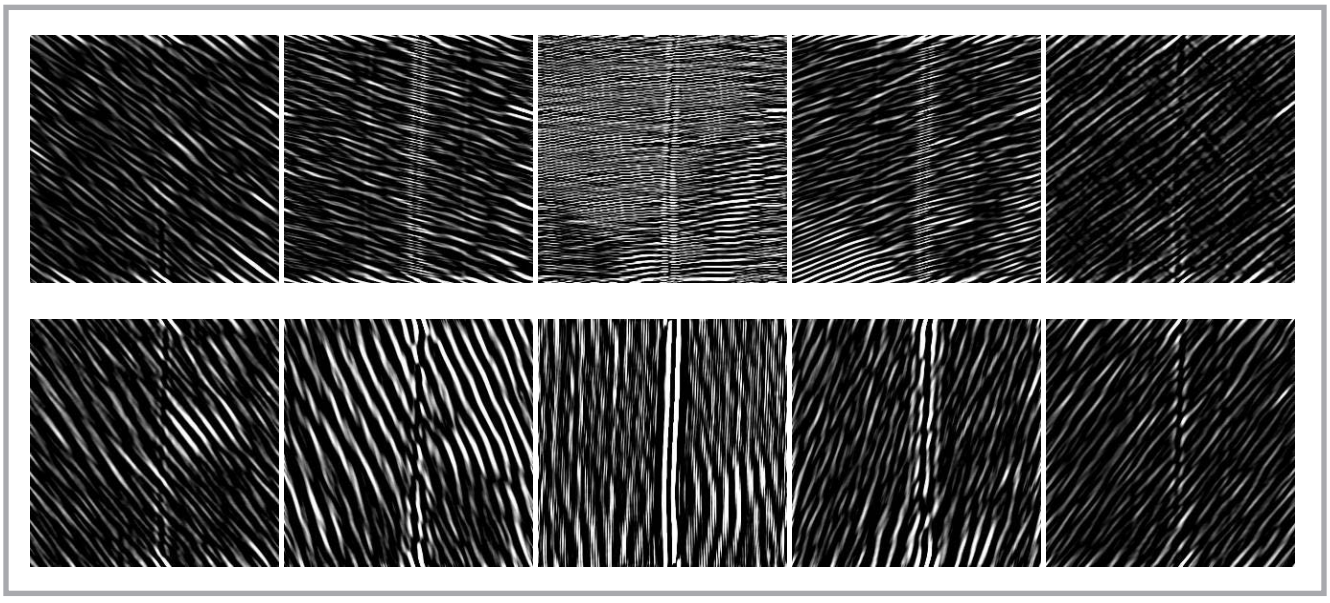

Figure 6. *Shearlet coefficients of the broken warp image at level 1.*

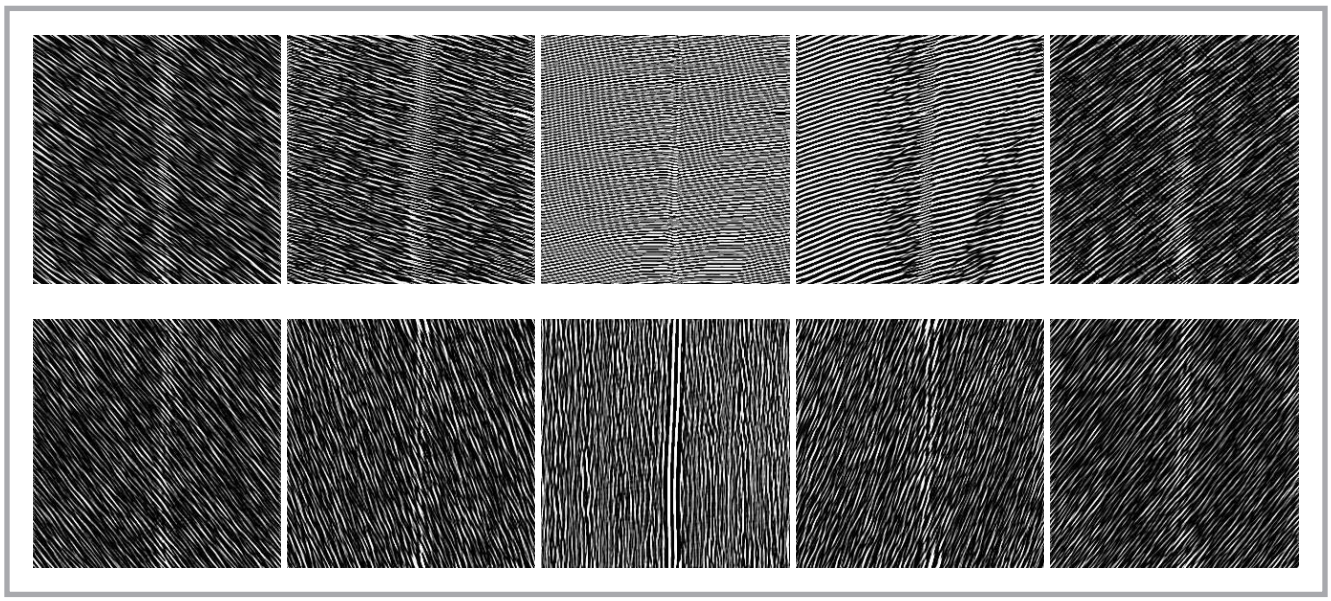

Figure 7. *Shearlet coefficients of the broken warp image at level 2.*

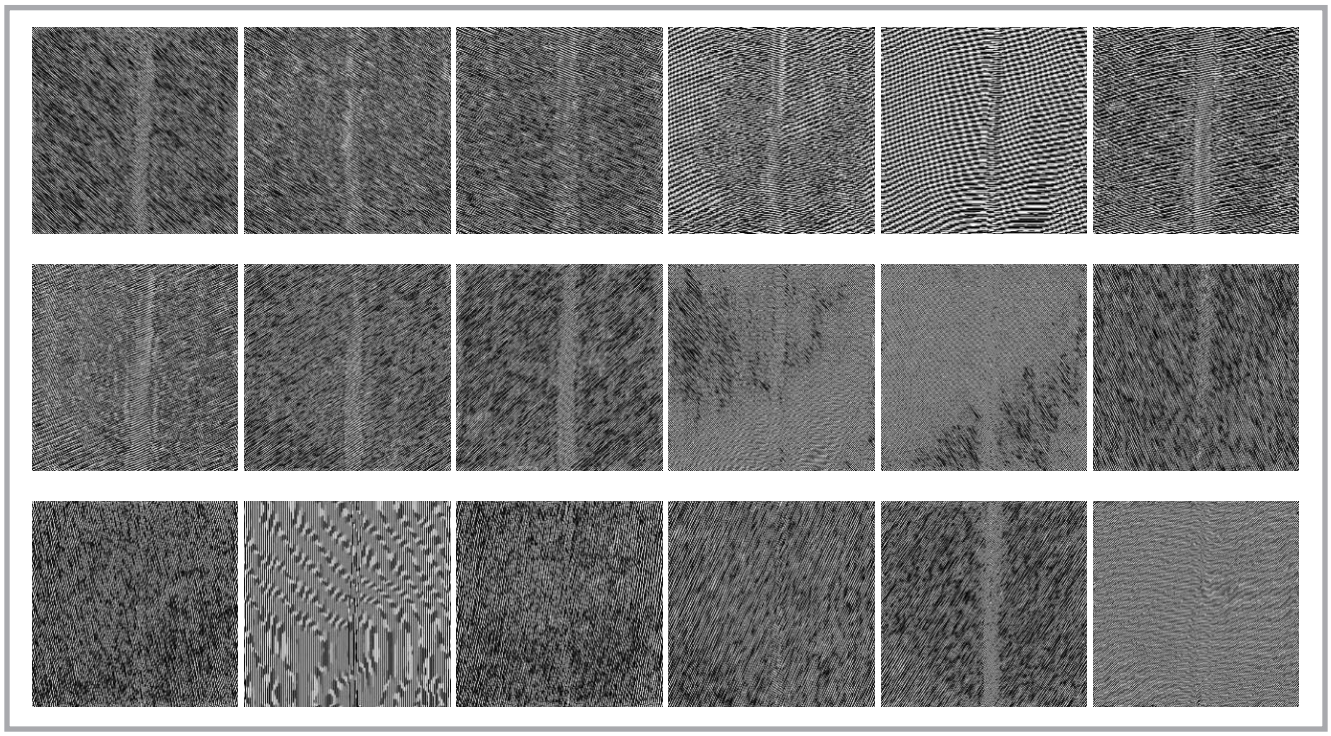

Figure 8. *Shearlet coefficients of the broken warp image at level 3.*

ed. In this work, when any of the remaining shearlet coefficients is larger than BE_A ($B \geq 2$), it will be defined as the signal coefficient and operated with the Rigrsure threshold rule. This method is relatively moderate. The calculation formulas of threshold T_R is shown as follows, where R_i is the ith element of risk-vector R and R_s is the smallest risk value.

$$R_i = \frac{\left| n - 2i - (n-i)E_i + \sum_{i=1}^{n} E_i \right|}{n} \quad (26)$$

$$T_R = \sigma\sqrt{R_s} \quad (27)$$

The last step of the segmented threshold de-nosing method is the Minimaxi threshold rule, applied for the remaining transition coefficients. Threshold T_M is illustrated as ***Equation (28)***, for which the notations have been explained before.

$$T_M = \begin{cases} \sigma\left(0.3936 + 0.1829\log_2 n\right) \\ 0 \end{cases} \quad (28)$$

After the steps of the decomposition with the segmented threshold de-nosing method is completed, most of the noise in these shearlet coefficients is removed, while keeping most of the edge information needed for reconstruction in the next procedure.

Reconstruction based on energy

De-noised shearlet coefficients at every level are obtained after the decomposition of the Sheralet transform with the segmented threshold de-noising method. Although these coefficients have been de-noised, it does not mean all of them are useful for the reconstruction of the high frequency at every level; those unnecessary shearlets coefficients should be removed to reconstruct promising

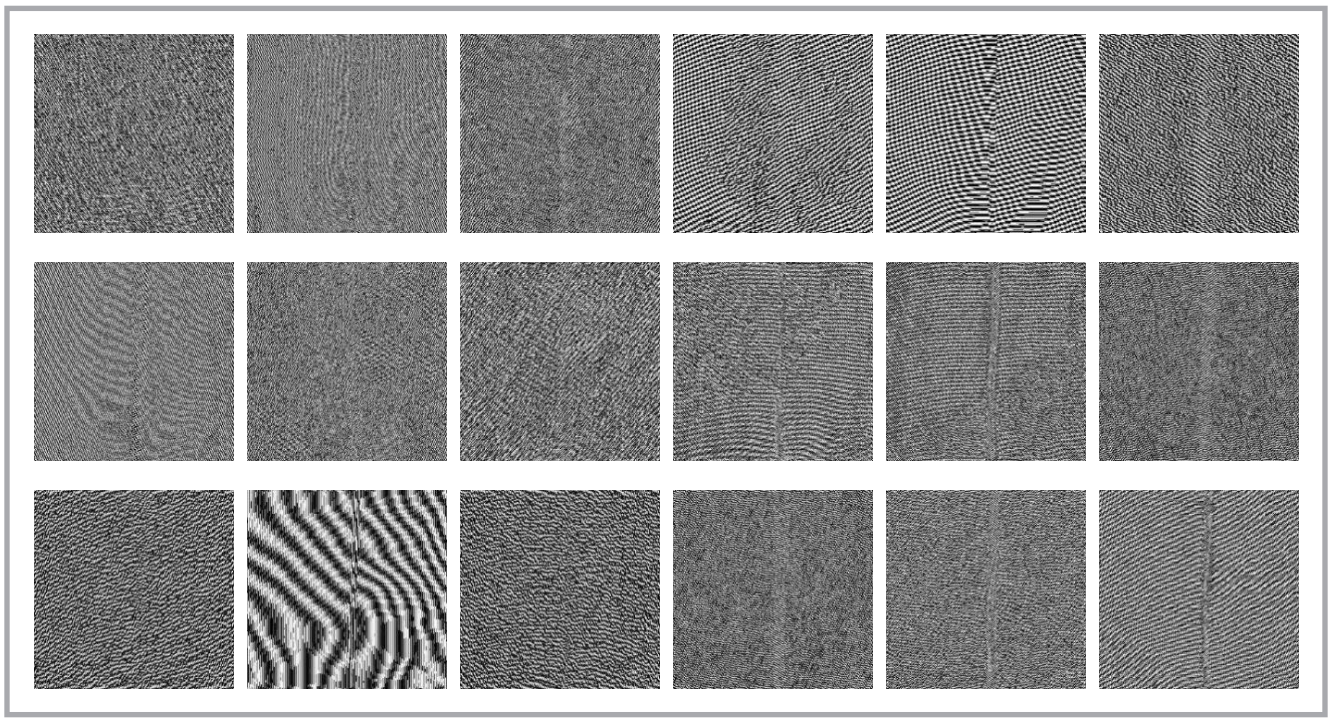

Figure 9. *Shearlet coefficients of the broken warp image at level 4.*

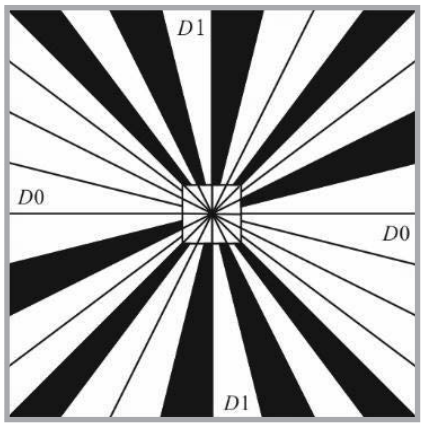

Figure 10. *Schematic graph of the shearlet coefficient selection.*

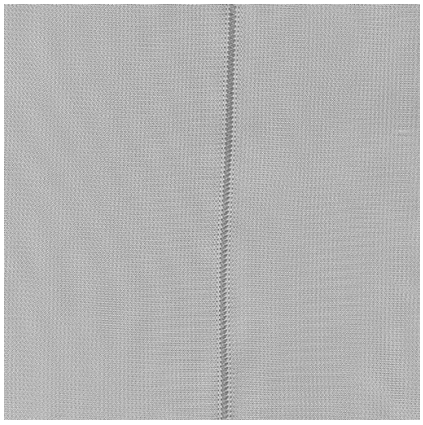

Figure 11. *Reconstructed image of warp-knitted fabric with broken warp.*

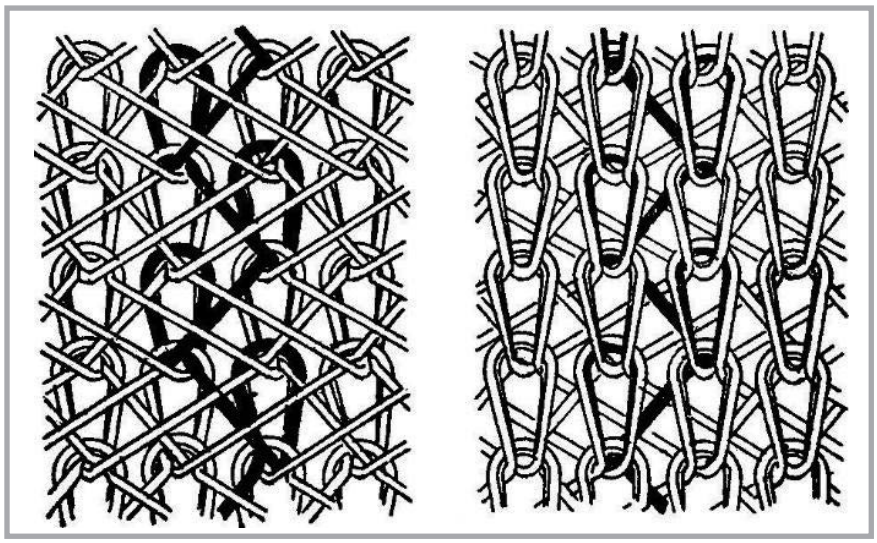

Figure 12. *Loop structure of warp-knitted fabric*

high frequency coefficients. In this work, valuable shearlet coefficients are selected using an energy method obtained based on ***Equation (24)***.

The selection rule for the values is illustrated as ***Equation (29)***. Where E_{al} is the average energy value of the lth level and $coeff_l^n$ is the nth shearlet coefficient of the lth level. The coefficient which is smaller than the average energy value E_{al} is set as the null coefficient matrix, and the rest coefficient is kept intact.

$$coeff_l^n = \begin{cases} coeff_l^n, & E_l^n \geq E_{al} \\ 0, & E_l^n < E_{al} \end{cases} \quad (29)$$

A schematic graph of the shearlet coefficient selection is shown in ***Figure 10***. The black regions are the coefficients selected, which will be used to recompose the high frequency coefficient of every level. Then the warp-knitted fabric image with a broken warp is reconstructed using the inverse discrete Shearlet transform, which is an inverse procedure of the decomposition. ***Figure 11*** shows the final reconstructed image of ***Figure 5***, which keeps most of the effective information due to the excellent properties of the Shearlet transform.

Iterative threshold segmentation and morphological operation

After the reconstructed fabric image is obtained, iterative threshold segmentation is needed for the next step. This

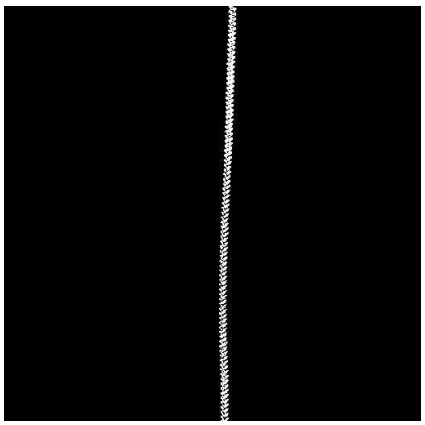

Figure 13. *Final result of the broken warp at the front bar.*

method is conventional, but its segmentation ability is excellent if the input image is of good quality. In the reconstructed image obtained above, the object is distinguished from the background, making the image suitable for segmentation by the iterative threshold method. The theory of this method can be expressed as ***Equation (30)***. Where T_1, T_O and T_B are the presupposed threshold, object threshold and background threshold, respectively; $f(i, j)$ is the gray value of the input image f and $P(i, j)$ is the probability of the gray value at point (i, j). When T_{k+1} is unchanged, the computation will be ended.

$$T_O = \frac{\sum_{f(i,j)<T_1} f(i,j) \times P(i,j)}{\sum_{f(i,j)<T_1} P(i,j)},$$

$$T_B = \frac{\sum_{f(i,j)>T_1} f(i,j) \times P(i,j)}{\sum_{f(i,j)>T_1} P(i,j)}, \quad (30)$$

$$T_{k+1} = \frac{T_O + T_B}{2}$$

However, the segmented result should also be processed by follow-up work in order to get a smoother result. In addition, the miscellaneous points generated by the loop structure of warp-knitted fabric should be eliminated. ***Figure 12*** shows the loop structure graph of the warp-knitted fabric of ***Figure 5***. The wispy loop holes will induce a dramatic gray level change, as does the defect . Because of this, the segmented result is not promising enough, and a great deal of little points are filled up. The morphological operations [25-26] are used to get rid of these points. Those whose area is smaller than the presupposed value will be removed. The miscellaneous points induced by the loop structure is far smaller than this value and will be removed completely. Then the image will be processed by the morphological opening to make the defect

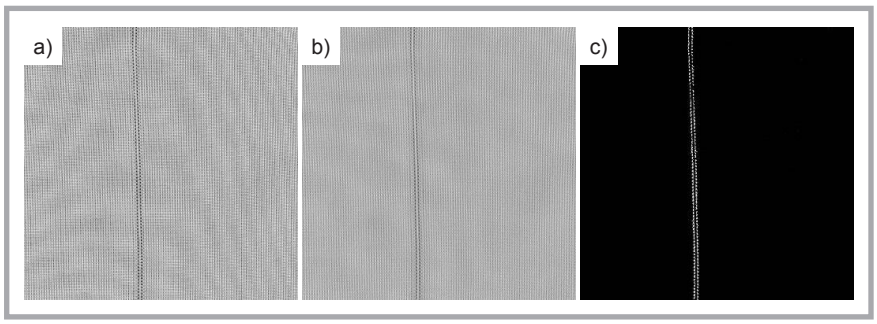

Figure 14. *Results of the broken warp at the back bar: a) original, b) reconstructed, c) result.*

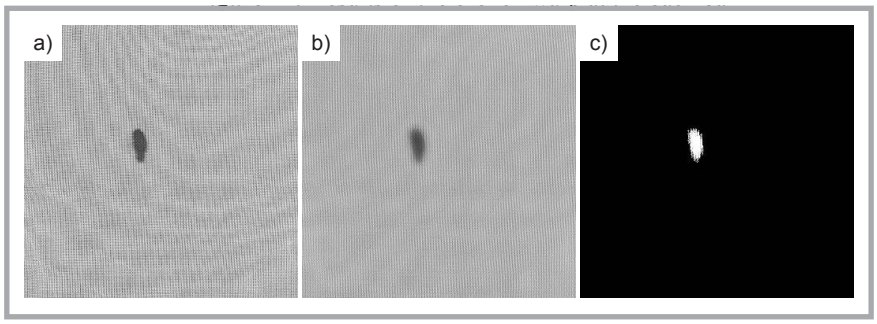

Figure 15. *Results of oil 2: a) original, b) reconstructed, c) result.*

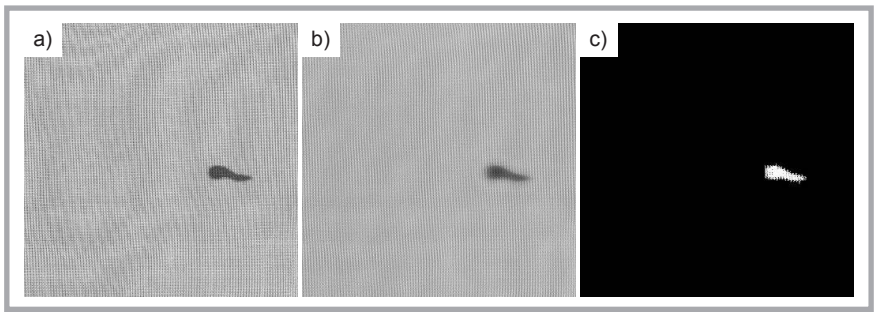

Figure 16. *Results of oil 2: a) original, b) reconstructed, c) result.*

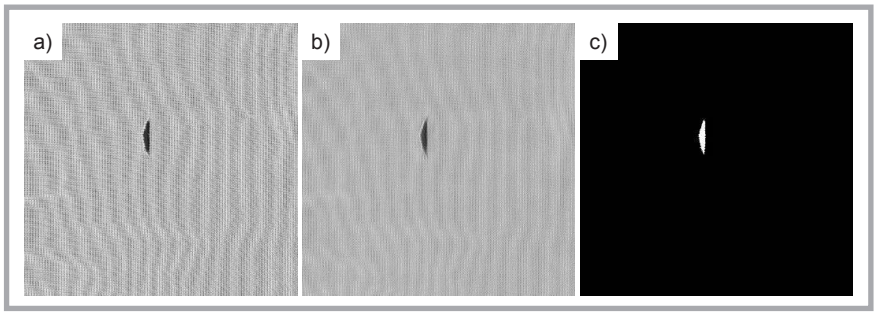

Figure 17. *Results of hole 1: (a) original, (b) reconstructed, (c) result.*

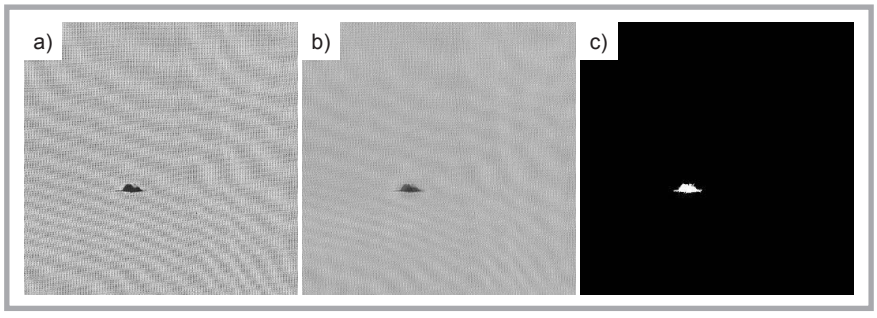

Figure 18. *Results of hole 2: a) original, b) reconstructed, c) result.*

object smooth. It is widely acknowledged that the theory of morphological opening is image erosion and dilation, which can make a large object smooth while erase tiny ones. Thus the final result is quite excellent; ***Figure 13*** shows the final image of the broken warp at the front bar.

Results

In order to investigate the performance of the method proposed above, preliminary experiments were performed on two-dimensional warp-knitted fabric images which had broken warp at the back bar, as well as oil 1, oil 2, hole 1 and hole 2, as shown in ***Figures 14-18.*** The original, reconstructed and segmented result images are shown in each of these Figures, respectively.

By comparing each segmented result with the original image, a segmented defect profile is obtained quite similar to the defect profile in the original image. These results maintain an accurate profile and demonstrates that the Shearlet transform with segmented threshold de-noising can keep most of directional information of the original images. Moreover from the results above we can also see that the final resultant image keeps most of the effective information of the warp-knitted fabric image and the defect in the fabric can be identified automatically, which demonstrates that it is an effective way to detect the defect in warp-fabric in the garment industry.

Conslusions

In this work we have introduced a burgeoning multiscale and geometric analysis method to detect defects on warp-knitted fabric, which are found based on the Shearlet transform. The method has a simpler discrete implementation than the Curvelet transform based on a rigorous and simple mathematical framework. It can provide more flexible decomposition on the basis of multiscale and geometric representation. Any number of shearlet coefficients can be obtained using this method.

After the acquisition of several groups of shearlet coefficients, these will be classified as the signal noise coefficient, transition coefficient and signal coefficient based on the energy and processed by the segmented threshold de-noising method. Then the promising shearlet coefficients are selected by energy selection to reconstruct high frequency coefficients, and the reconstructed image will be formed by the inverse Shearlet transform. The final segmented result is obtained through the iterative threshold segmentation and morphological operation. The results demonstrate that the segmented defect profile is quite distinct and verisimilar compared with the original fabric defect images. It can be applied in further automatic warp-knitted fabric defect identification.

Acknowledgements

The authors acknowledge the financial support from the National Science Foundation of China (No.11302085 and No.51403080), Fundamental Research Funds for the Central Universities (No. JUSRP51625B), and the Innovation fund project of Cooperation among Industries, Universities & Research Institutes of Jiangsu Province (No. BY2016022-42).

References

1. Jiang GM. *Production technology of warp-knitted fabric-warp knitting theory and typical products*.1st edn. Beijing: China Textile & Apparel Press, 2010: 1-3.
2. Ngan HYT, Pang GKH, Yung NHC. Automated fabric defect detection – A review. *Image & Vision Computing* 2011; 29(7): 442-458.
3. Haralick RM. Statistical and structural approaches to texture. *Proceedings of the IEEE* 1979, 67(5): 786-804.
4. Haralick RM, Shanmugam K, Dinstein I. Textural Features for Image Classification. *Systems Man & Cybernetics IEEE Transactions on*, 1973, smc-3(6): 610-621.
5. Serra J. *Image Analysis and Mathematical Morphology*. Academic Press, Inc., 1982.
6. Conci A, Proença CB. A fractal image analysis system for fabric inspection based on a box-counting method. *Computer Networks & Isdn Systems* 1998; 30(98): 1887-1895.
7. Han Y, Shi P. An adaptive level-selecting wavelet transform for texture defect detection. *Image & Vision Computing* 2007; 25(8): 1239-1248.
8. Castellini C, Francini F, Longobardi G, et al. On-line textile quality control using optical Fourier transforms. *Optics & Lasers in Engineering* 1996; 24(1): 19-32.
9. Liu X, Su Z, Wen Z, et al. Slub Extraction in Woven Fabric Images Using Gabor Filters. *Textile Research Journal* 2008; 78(4): 320-325.
10. Hajimowlana SH, Muscedere R, Jullien G A, et al. 1D autoregressive modeling for defect detection in web inspection systems. Circuits and Systems. *1998. Proceedings. 1998 Midwest Symposium on. IEEE*, 1998: 318-321.
11. Ozdemir S, Ercil A. Markov random fields and Karhunen-Loeve transforms for defect inspection of textile products. Emerging Technologies and Factory Automation, 1996. *EFTA '96. Proceedings., 1996 IEEE Conference on. IEEE*, 1996: 697-703.
12. Kumar A. Neural network based detection of local textile defects[J]. *Pattern Recognition* 2003; 36(7):1645-1659.
13. Bodnarova A, Bennamoun M, Kubik K K. Defect detection in textile materials based on aspects of the HVS. *Systems, Man, and Cybernetics, 1998. 1998 IEEE International Conference on. IEEE*, 1998: 4423-4428 vol.5.
14. Bodnarova MBA. Digital Image Processing Techniques for Automatic Textile Quality Control. *Systems Analysis Modelling Simulation* 2003; volume 43(11): 1581-1614.
15. Ngan HYT, Pang GKH, Yung NHC. Ellipsoidal decision regions for motif-based patterned fabric defect detection. *Pattern Recognition* 2010; 43(6): 2132-2144.
16. Kingsbury N. Complex Wavelets for Shift Invariant Analysis and Filtering of Signals. *Applied & Computational Harmonic Analysis* 2001; 10(3): 234-253.
17. Meyer FG, Coifman RR. Brushlets: A Tool for Directional Image Analysis and Image Compression. *Applied & Computational Harmonic Analysis* 1997, 4(2): 147-187.
18. Candès EJ, Donoho DL. *Ridgelets: A Key to Higher-Dimensional Intermittency?* Philosophical Transactions of the Royal Society of London, 1999, 357(1760): 2495.
19. Candès EJ, Donoho DL. New tight frames of curvelets and optimal representations of objects with C2 singularities. *Communications on Pure & Applied Mathematics* 2004; 57: 219-266.
20. Do MN, Vetterli M. The contourlet transform: an efficient directional multiresolution image representation. IEEE Trans Image Process. *IEEE Transactions on Image Processing* 2006; 14: 2091-2106.
21. Easley G, Labate D, Lim W Q. Sparse directional image representations using the discrete shearlet transform. *Applied & Computational Harmonic Analysis* 2008, 25(1): 25-46.
22. Guo K, Labate D. Optimally sparse multidimensional representation using shearlets. *SIAM J. Math. Anal.* 39, 298-318.
23. Guo K, Labate D, Lim W Q, et al. Wavelets with composite dilations and their MRA properties. *Applied & Computational Harmonic Analysis* 2006; 20(2): 202-236.
24. Dou J, Li J. Optimal image-fusion method based on nonsubsampled contourlet transform. *Optical Engineering* 2012; 51(10): 2002-2009.
25. Gonzalez RC, Woods RE, Eddins SL. *Digital Image Processing Using MATLAB*. Pearson Education India, 2004: 334-377.
26. Gonzalez RC, Woods RE. *Digital Image Process*, Third Edition. Pearson Education India, 2010: 649-702.
27. Vivek C, Audithan S. Colour Texture Image Analysis by Shearlets. *J. Applied Sci.* 2014; 14: 697-702.

Received 22.01.2016 Reviewed 26.06.2017